

Mass-Transfer Process of Galactic Compact Binaries

Zi-han Zhang^{1,*}, Bin Liu^{1,†}, Sheng-hua Yu², and Jie Yang^{1,3,4,5‡}

¹*School of Physical Science and Technology, Lanzhou University, Lanzhou 730000, China*

²*CAS Key Laboratory of FAST, National Astronomical Observatories,
Chinese Academy of Sciences, 20A Datun Road, Beijing 100101, China*

³*Institute of Theoretical Physics & Research Center of Gravitation, Lanzhou University, Lanzhou 730000, China*

⁴*Key Laboratory of Quantum Theory and Applications of MoE,
Lanzhou University, Lanzhou 730000, China and*

⁵*Lanzhou Center for Theoretical Physics & Key Laboratory of Theoretical
Physics of Gansu Province, Lanzhou University, Lanzhou 730000, China*

(Dated: June 13, 2023)

In this paper, we focus on the effect of mass-transfer between compact binaries like neutron-star—neutron-star (NS-NS) system and neutron-star—white-dwarf (NS-WD) system. We adopt the mass quadrupole formula with post-Newtonian approximation to calculate the gravitational wave (GW) radiation and the orbital evolution. Two kinds of mass-transfer processes are considered here. One is the tidal disruption model where the less dense star orbits into the other one's Roche limit and its mass flows toward the more compact star as a beam of incompressible fluid. The other is common envelope evolution model. We divide the mass-loss of the companion star into the mass-inflow to the primary star and the mass-background winding in the Roche lobe of the primary star. Viewing this envelope as a background, the GW of its spin can be calculated as a rotating non-spherically symmetric star. Assuming a mass-inflow parameter α , we eventually obtained the radiation power and the GWs strain, then corrected gravitational wave form (GWF) templates for different initial mass ratios in the inspiral phase.

I. INTRODUCTION

The galactic compact binaries are important sources of celestial GW detection [1, 2]. They are within the sensitive frequency band (0.1 mHz \sim 0.1 Hz) of detectors and they are rich in number [3]. GW signals from these sources contain a wealth of information about their formation and evolution, mass transfer, and the equation of state [4]. Establishing an accurate gravitational wave form (GWF) template library for close compact binary stars with Roche lobe overflow, material exchange, and other influences can not only help to analyze waveforms, but also benefit data processing for numerous compact binaries. Along with that, when searching for other outer galactic objects we are interested in, noises from inner compact binaries can be reduced [5–9].

The strain and frequency of GWs vary from different compact gravitational wave sources, which commonly include BH-BH, BH-NS, NS-NS, NS-WD, and WD-WD [10]. The GWs of Extreme Mass-Ratio Inspirals (EMRI) and Compact Binary Coalescence (CBC) are research hotspots of this field and have been widely studied. The current terrestrial detectors like LIGO and Virgo, along with celestial detectors like LISA, TaiJi, TianQin, and DECIGO [11–13], have different sensitivity in the strain and frequency domain. Thus, corresponding GW templates are required as a priority to determine the detec-

tion band. For NS-NS and NS-WD binaries, the detection distance is at the order of 10^2 Mpc [14, 15], and we are expected to detect several or dozens of NS-NS merger signals in the future.

The post-Newtonian approximation [16–20] is widely used in the approximate solutions of the Einstein field equation, expanding it to higher order terms than Newtonian to make the solution more precise. It plays a significant role in the theoretical calculation of GWs from slow-moving objects in weak fields, which are the most cases in binary systems. The theoretical framework of post-Newtonian approximation approach to a binary system consists of two parts: binary dynamics and GW emissions [21]. The post-Newtonian dynamical equations of this two-body problem generally take two forms [22]: the Hamiltonian form and the Lagrangian form. In some situations, the Lagrangian form may give chaotic orbits, while the latter is always compatible with Keplerian-type parametric solutions that we are used to. These are also crucial parameters in calculating the GWF of binaries inspiralling along post-Newtonian accurate eccentric orbits [23]. So our procedure is to first solve the dynamics equations, and then plug the orbit into GW formula to obtain the waveform.

GW signals generated by the inspiral and merger of binary stars are the main targets of future celestial GW detectors. This paper discusses the evolution of NS-NS and NS-WD binary systems in the context of general relativity and calculates their GWFs using the post-Newtonian approximation. Notice that the mass range of NSs is generally between $1.35 \sim 2.1 M_\odot$, and the radius is between $1.4 \times 10^{-5} \sim 3.3 \times 10^{-5} R_\odot$, while WDs are much looser with a mass range generally between $0.4 \sim 1.2 M_\odot$, and

* zhangzihan19@lzu.edu.cn

† liubin2020@lzu.edu.cn

‡ Corresponding author: yangjiev@lzu.edu.cn

radius between $8 \times 10^{-3} \sim 2 \times 10^{-2} R_\odot$, so more attention is paid on the NS-WD binaries when we investigate the effect of mass-transfer [24–26].

As for the outcome of NS-NS merger, it varies depending on the angular momentum, mass ratio, equation of state, and other conditions. Usually, the total mass of an inner Milky Way NS-NS binary is within $2.5 \sim 2.88 M_\odot$, and the mass ratio is between 1.1 and 1.3. When the total mass reaches $3.15 \sim 4.10 M_\odot$, the binary may immediately collapse into a black hole with angular momentum density $a = J/M$ around $0.7 \sim 0.8$ [27, 28]. The material of its accretion disk will eventually fall into the black hole along with the GW radiation and angular momentum loss in the ringdown phase. That is the situation we take into consideration at the end of evolution, whose GW can be calculated by black hole perturbation theory.

The theoretical analysis and numerical computation in this paper are arranged in the following sections. In Sec.II, we briefly review the standard routine to simplify the independent variables in Einstein field equation in the TT gauge where the final metric perturbation $h_{\mu\nu}$ has only two independent variables $h_+(t)$ and $h_\times(t)$. In Sec.III, we give the evolution equation of the binary system and use post-Newtonian approximation of Hamiltonian form to calculate the trajectory and radiation power. In Sec.IV, we propose the tidal disruption model [29–31], and common envelope model [32, 33], where the GW of the mass-background is treated as a rotating non-spherically symmetric star[34, 35]. Finally, waveforms with respect to different mass-inflow parameters and initial mass ratios are discussed. All calculations are in natural units where $G = c = 1$.

II. TWO POLARIZATION MODES

We begin with the Einstein field equation, where the metric $g_{\mu\nu}$ is a symmetric (0,2) tensor with generally 10 independent variables constrained by 10 correlated second-order nonlinear partial differential equations

$$G_{\mu\nu}(g_{\mu\nu}) = \kappa T_{\mu\nu}. \quad (1)$$

Due to the conservation of energy-momentum tensor, 4 constrains are eliminated by Bianchi identity

$$\nabla^\mu G_{\mu\nu} = 0. \quad (2)$$

The independence of coordinates also loses 4 constrains, leaving only two constrains with actual physical meaning. To obtain the specific metric with those two variables, supplemental constrains are required along with Einstein field equation, which are the harmonic gauge and Transverse-Traceless (TT) gauge [36] as

$$h_{ij}^{TT} = h_{ji}^{TT}, \quad \sum_i h_{ii}^{TT} = 0, \quad \sum_i \nabla_i h_{ij}^{TT} = 0. \quad (3)$$

Writing down the spacetime metric as $g_{\mu\nu} = \eta_{\mu\nu} + h_{\mu\nu}$,

where $\eta_{\mu\nu}$ is the flat metric and $h_{\mu\nu}$ are small perturbations, the former reduces Einstein field equation to

$$\square \tilde{h}_{\mu\nu} = -2\kappa T_{\mu\nu}, \quad \tilde{h}_{\mu\nu} = h_{\mu\nu} - \frac{h}{2}\eta_{\mu\nu}. \quad (4)$$

Choosing the GW transverses to z axis, the latter gives

$$h_{ab}^{TT}(t, z) = \begin{pmatrix} C_+ & C_\times \\ C_\times & -C_+ \end{pmatrix} \cos[\omega(t - \frac{z}{c})], \quad (5)$$

where $a, b = 1, 2$, z is the direction of propagation, and C is the time independent strain of GW. Set $h_{ab} \equiv C_{ab} \cdot \cos[\omega(t - \frac{z}{c})]$, then we can get the metric

$$ds^2 = -c^2 dt^2 + dz^2 + (1 + h_+)dx^2 + (1 - h_+)dy^2 + 2h_\times dx dy. \quad (6)$$

Based on this metric, we can get the equation of $h_+(t)$ and $h_\times(t)$ by calculating the perturbation of metric tensor.

III. BINARIES' EVOLUTION AND GWF

A. Mass Quadrupole Tensor

We use $[M]$ to measure time, length, and mass in natural units. The masses of the two stars are m_1 and m_2 respectively where $m_1 \geq m_2$. Setting the rotation plane to be xOy plane, we calculate the mass quadrupole tensor and its third-order derivative.

$$\ddot{Q}_{xx} = \beta b(2 \sin 2\theta + 3e \sin \theta \cos^2 \theta), \quad (7)$$

$$\ddot{Q}_{yy} = -\beta b[2 \sin 2\theta + e \sin \theta(1 + 3 \cos^2 \theta)], \quad (8)$$

$$\ddot{Q}_{xy} = \ddot{Q}_{yx} = -\beta b[2 \cos 2\theta - e \cos \theta(1 - 3 \cos^2 \theta)] \quad (9)$$

where e is the eccentricity, θ is the anomaly, a is the winding semi-major axis, and $b \equiv (1 + e \cos \theta)^2$. And we have

$$\dot{\theta} = \frac{[(m_1 + m_2)a(1 - e^2)]^{\frac{1}{2}}}{r^2}, \quad (10)$$

$$\beta^2 \equiv \frac{4m_1^2 m_2^2 (m_1 + m_2)}{a^5 (1 - e^2)^5}. \quad (11)$$

The radiation power P only depends on \ddot{Q} :

$$P = -\frac{dE}{dt} = \frac{1}{5}(\ddot{Q}_{ij}\ddot{Q}^{ij} - \frac{1}{3}\ddot{Q}_i{}^i\ddot{Q}_j{}^j). \quad (12)$$

According to the expression of the mass quadrupole tensor, we can get the average radiation power in a period

$$\bar{P} = \frac{32}{5} \frac{m_1^2 m_2^2 (m_1 + m_2)}{a^5 (1 - e^2)^{\frac{7}{2}}} (1 + \frac{73}{24}e^2 + \frac{37}{96}e^4). \quad (13)$$

B. Post-Newtonian Approximation

Usually the pressure and temperature are negligible for regular compact binaries in weak fields [16, 37]. Here we only consider the dynamic equations of compact binaries due to mass distribution. Parameters are introduced as: the total mass of system $M = m_1 + m_2$, the lost mass $\delta m = m_2^{(0)} - m_2$ of m_2 , where $m_2^{(0)}$ is the initial mass of star 2 and m_2 is the final mass. $\mu = m_1 m_2 / M$, $\nu = (m_1 - m_2) / M$, and $\eta = (1 - \nu^2) / 4$, $q = m_1 / m_2$. Let \mathbf{x} and \mathbf{v} be the relative coordinate vector and velocity vector, defining the unit vector $\mathbf{n} = \mathbf{x} / r$ where r is the distance between two stars.

These post-Newtonian dynamics equations for the two-body problem have can be written as Hamiltonian form or Lagrangian form [22]. In harmonic gauge, the expansion of acceleration \mathbf{a} of Lagrangian form is

$$\mathbf{a} = \mathbf{a}_N + \mathbf{a}_{PN}^{(1)} + \mathbf{a}_{PN}^{(2)} + \mathbf{a}_{PN}^{(2.5)}, \quad (14)$$

the expressions of \mathbf{a} can be found in citations [38–40].

$$\begin{aligned} \mathbf{a}_{PN}^{(2.5)} = & \frac{8}{5} \left(\frac{\eta}{r} \right) \left\{ \frac{\mathbf{n}}{r} [(\mathbf{r} \cdot \mathbf{p}) \left(\frac{17}{13r} + 3p^2 + \frac{9}{2}(3\eta - 1)p^4 \right) \right. \\ & - \frac{1}{2} \left(5\eta + \frac{179}{3} \right) \frac{p^2}{r} - \frac{1}{3} (25\eta + 51) \frac{1}{r^2} - 6\eta \frac{(\mathbf{n} \cdot \mathbf{p})^2}{r} \left. \right] \\ & - \frac{\mathbf{p}}{r^2} \left[\frac{3}{r} + p^2 + \frac{3}{2}(3\eta - 1)p^4 + \frac{1}{2}(3\eta - 21) \frac{p^2}{r} \right. \\ & \left. \left. - 3(3 + \eta) \frac{1}{2} - 2\eta \frac{(\mathbf{n} \cdot \mathbf{p})^2}{r} \right] \right\} \end{aligned} \quad (15)$$

Here we choose Hamiltonian to avoid chaotic results by Lagrangian form [41]. The conserved 2.5PN Hamiltonian in the relative coordinate is

$$\mathcal{H}(\mathbf{r}, \mathbf{p}) = \mathcal{H}_N + \mathcal{H}_{PN}^{(1)} + \mathcal{H}_{PN}^{(2)}. \quad (16)$$

To obtain the trajectory of binaries, we need to calculate high order expansions of Hamiltonian equations [42, 43], the derivatives of \mathcal{H} respective to the total momentum p are

$$\frac{\partial \mathcal{H}}{\partial p_N} = p, \quad (17)$$

$$\frac{\partial \mathcal{H}^{(1)}}{\partial p_{PN}} = \frac{1}{2} (3\eta - 1) p^3 - \frac{1}{2} [(3 + \eta) 2p + \eta \cos \phi] \frac{1}{r}, \quad (18)$$

$$\begin{aligned} \frac{\partial \mathcal{H}^{(2)}}{\partial p_{PN}} = & \frac{1}{4} (1 - 5\eta + 5\eta^2) p^3 + \frac{1}{4} [-8\eta^2 p^3 \cos^2 \phi \\ & + (5 - 20\eta - 3\eta^2) p^2 - 12\eta^2 p^3 \cos^4 \phi] \frac{1}{r} \\ & + \frac{1}{2} [(5 + 8\eta) 2p + 6\eta \cos^2 \phi] \frac{1}{r^2}, \end{aligned} \quad (19)$$

and those respective to r are

$$\frac{\partial \mathcal{H}}{\partial r_N} = \frac{1}{r^2}, \quad (20)$$

$$\frac{\partial \mathcal{H}^{(1)}}{\partial r_{PN}} = \frac{1}{2} [(3 + \eta) p^2 + \eta p \cos \phi] \frac{1}{r^2} - \frac{1}{r^3}, \quad (21)$$

$$\begin{aligned} \frac{\partial \mathcal{H}^{(2)}}{\partial r_{PN}} = & -\frac{p^2}{8r^2} [(5 - 20\eta - 3\eta^2) - 2\eta^2 p^2 \cos^2 \phi \\ & - 3\eta^2 p^2 \cos^4 \phi] + [(5 + 8\eta) p^2 \\ & + 3\eta p^2 \cos^2 \phi] \frac{1}{r^3} - \frac{3}{4} (1 + 3\eta) \frac{1}{r^4}, \end{aligned} \quad (22)$$

where ϕ is the angular separation between \mathbf{r} and \mathbf{p} , imply $\mathbf{r} \cdot \mathbf{p} = rp \cos \phi$. Those dynamical equations are highly nonlinear partial differential equations, which are difficult to solve analytically [44], so we turn to numerical solutions.

C. Gravitational Wave Form

In order to obtain the complete GWF, we consider binaries merge to form a black hole. The evolutionary process of binary systems can be generally divided into three phases as inspiral-merger-ringdown. The GW h^{IM} during inspiral and merger can be calculated by post-Newtonian approximation, and that of ringdown h^{RD} calculated by black hole perturbation theory [45], where t_0 is the time of merger.

$$h = h^{IM} \Theta(t_0 - t) + h^{RD} \Theta(t - t_0), \quad (23)$$

where Θ is jump function of t . if $t_0 - t > 0$, then $\Theta(t_0 - t) = 1$, for the else $\Theta(t_0 - t) = 0$. In late ringdown trailing phase, we have [46–48]:

$$h^{RD} = \frac{8\mu}{R} \sqrt{\frac{\pi}{5}} e^{-im\phi} H^{RD}, \quad (24)$$

where R is the distance from the source, and for the GW150914 we have $R = 1.768 \times 10^{20} R_\odot$. When it is far enough the above equation can be approximated as

$$h^{RD} = \frac{8\mu}{R} \sqrt{\frac{\pi}{5}} e^{-\frac{\pi f t}{Q}} \cos(2\pi f t), \quad (25)$$

$$Q = 2(1 - a_*)^{-\frac{9}{20}} = 2(1 - \frac{cJ}{GM^2})^{-\frac{9}{20}}, \quad (26)$$

$$a_* = cJ/GM^2 = \mathbf{J}/M^2, \quad (27)$$

a_* is the spin rate of black hole [49]. The angular momentum $\mathbf{J} = \mathbf{r}_i \cdot \mathbf{p}_i$, where \mathbf{r}_i , \mathbf{p}_i is the winding radii and momentum of binaries. The usual compact binary systems in the Milky Way, GS2000+25 and LMC X-3 systems, their spin rate $a_* = 0.03$ [50].

The Newman-Penrose formalism can be obtained from the two independent polarization modes h_\times and h_+ . At infinity from the wave source, all gravitational radiative degrees of freedom are contained a master wave equation

of the Weyl scalars ψ_n ($n = 0, 1, 2, 3, 4$) [51, 52], where only ψ_4 remains in significance

$$\psi_4(t) = \frac{\partial^2}{\partial t^2}(h_+(t) - ih_\times(t)), \quad (28)$$

It indicates that the complex Weyl scalar ψ_4 are determined by the second derivative of h_+ and h_\times with respect to time.

We use the mass quadrupole tensor to express h_{ij} with higher-order expansions of \mathcal{H} [53].

$$h_{ij} = \frac{2\mu r}{R} [\mathcal{H}_{ij}^{(0)} + r^{1/2}\mathcal{H}_{ij}^{(1/2)} + r^1\mathcal{H}_{ij}^{(1)} + r^{3/2}\mathcal{H}_{ij}^{(3/2)} + r^2\mathcal{H}_{ij}^{(2)} + \mathcal{O}(\frac{1}{c^5})]_{TT}. \quad (29)$$

The two polarization modes of GW [54] are

$$h_+(t) = \frac{4\mathcal{M}^{\frac{5}{3}}}{R} M^{\frac{1}{3}} \frac{1 + \cos^2 \psi}{2r(1 - e^2)} \cos(2\pi f_{GW}t + 2\varphi), \quad (30)$$

$$h_\times(t) = \frac{4\mathcal{M}^{\frac{5}{3}}}{R} M^{\frac{1}{3}} \frac{\cos \psi}{r(1 - e^2)} \sin(2\pi f_{GW}t + 2\varphi), \quad (31)$$

where ψ is the deflection angle of binaries and f_{GW} is the radiation frequency of GW [23, 55], which is mainly determined by chirp mass $\mathcal{M} = (m_1 m_2)^{3/5} M^{-1/5}$ and $\tau = t - t_0$.

$$f_{GW}(\tau) = \frac{1}{8\pi} \left(\frac{5}{\tau}\right)^{\frac{3}{8}} \mathcal{M}^{-\frac{5}{8}} \quad (32)$$

The frequency of GW is twice of inspiral frequency $f_{GW} = 2f$. Since mass-transfer mainly happens in inspiral and merger, our discussion on the GWF and binary evolution correction are focus ed on that period. To make the whole process more complete, we extend our GWF to ringdown phase h^{RD} , which also varies as the mass-transfer correction is applied to common envelope evolution mode.

D. Binary System Evolution Equations

Based on the results above, we set the gravitational potential E , winding frequency f , and rotation period T as functions of time. Plugging into formulas we obtain the radiation power P and the waveform of h_+ and h_\times . Furthermore, we draw the trajectory of binary stars according to their radii r_1 and r_2 .

The convergent canonical Hamiltonian equations are

$$\frac{dr}{dt} = \frac{\partial \mathcal{H}}{\partial p}, \quad (33)$$

$$\frac{dp}{dt} = -\frac{\partial \mathcal{H}}{\partial r} + a_{PN}^{(2.5)}. \quad (34)$$

The dissipation term of 2.5PN leads to the Hamiltonian of the system is not conservative. From that we have

evolution equations of orbit parameters taking spin $\mathbf{S} = 0$ in Eulerian form[56, 57]

$$\frac{da}{dt} = -\frac{64}{5} \frac{\mu M^2}{a^3(1 - e^2)^{\frac{7}{2}}} \left(1 + \frac{73}{24}e^2 + \frac{37}{96}e^4\right), \quad (35)$$

$$\frac{de}{dt} = -\frac{304}{15} \frac{e\mu M^2}{a^4(1 - e^2)^{\frac{5}{2}}} \left(1 + \frac{121}{304}e^2\right), \quad (36)$$

$$\frac{dE}{dt} = -\frac{8}{15} \frac{m_1^2 m_2^2 M}{a^5(1 - e^2)^5} b^4 (12b^2 + e^2 \sin \theta), \quad (37)$$

$$\frac{dT}{dt} = -\frac{96}{5} \frac{T\mu M^2}{a^4(1 - e^2)^{\frac{7}{2}}} \left(1 + \frac{73}{24}e^2 + \frac{37}{96}e^4\right). \quad (38)$$

Here we set the initial values as

$$\begin{aligned} m_1 &= 2M_\odot, \quad m_2 = 1.4M_\odot, \\ a &= r = 25R_\odot, \\ R &= 1.8 \times 10^{18} R_\odot, \\ |v_0| &= 1 \times 10^{-4}, \\ \theta &= 0, \\ e &= 0.1, 0.3, 0.6. \end{aligned}$$

4th-order Rounge-Kutta method is used to numerically solve those differential equations. The GWFs are shown as follows by plugging data into formulas. A comparative figure of different initial eccentricities of NS-NS binaries without mass-transfer is given in FIG.1.

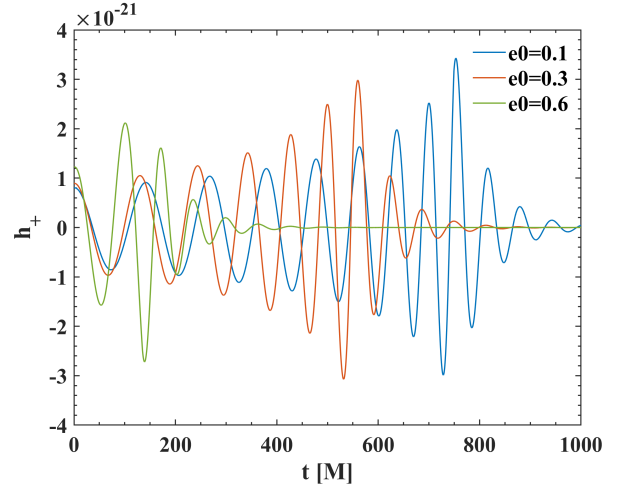


FIG. 1. The figure shows GWs with different initial eccentricities $e = 0.1, 0.3, 0.6$. Fixing the initial distance, when the eccentricity gets larger, binaries tend to merge more quickly with a smaller amplitude and larger frequency. In extremity, two stars straightly collide at maximum eccentricity, taking the shortest time and nearly no GW is emitted, meaning the smallest amplitude.

In order to better reflect the evolution of the binary motion equation and the corresponding GWF at this initial distance, we will take $e = 0.3$ as the initial eccentricity in the subsequent calculation.

IV. MASS TRANSFER CORRECTION

A. Mass Quadrupole Correction

We establish a model where there is a stable and conservative mass-loss flow between two stars, whose quadrupole tensor can be written as

$$Q'_{ij} = \frac{m_0}{3} \left[1 - \frac{3m_1 m_2}{M^2} \right] L^2 W \omega, \quad (39)$$

$$W_{ab} = \begin{pmatrix} \cos 2\theta & \sin 2\theta \\ \sin 2\theta & -\cos 2\theta \end{pmatrix}, \quad \varphi \equiv 2\theta, \quad (40)$$

$$\ddot{W}_{ab} = \begin{pmatrix} -\ddot{\varphi} \sin \varphi - \dot{\varphi}^2 \cos \varphi & \ddot{\varphi} \cos \varphi - \dot{\varphi}^2 \sin \varphi \\ \ddot{\varphi} \cos \varphi - \dot{\varphi}^2 \sin \varphi & \ddot{\varphi} \sin \varphi + \dot{\varphi}^2 \cos \varphi \end{pmatrix}, \quad (41)$$

$$\ddot{Q}'_{ij} \approx \frac{m_0}{3} L^2 \ddot{W}, \quad \ddot{Q}_{ij} = \ddot{Q}_{ij}^0 + \ddot{Q}'_{ij}, \quad (42)$$

where Q_{ij}^0 is the mass quadrupole of the two stars without mass-transfer, and L is length of the mass-transfer flow.

Here we propose the following two models of mass-transfer: the tidal disruption model and the common envelope evolution model, which are illustrated in FIG. 2. We set the value of mass-loss as δm_l , mass-inflow as δm_i , mass-background as δm_b , and $\delta m_l = \delta m_i + \delta m_b$.

B. Tidal Disruption

Considering a straight in-compressible flow of mass-loss from m_2 star to m_1 star in the Roche limit of the more massive star, where the mass flow deposits on m_1 vary rapidly. In order to represent the strength of the mass-transfer, we introduced the Euler equations for in-compressible fluids [58, 59].

$$\frac{dm_2}{dt} = \frac{dm_2}{dv} \cdot \frac{dv}{dt} = \frac{dV}{dv} \cdot \rho \frac{dv}{dt} = \frac{1}{\delta v} F_T, \quad (43)$$

$$\rho \frac{dv}{dt} = -\nabla P_p + \rho \tilde{g}, \quad (44)$$

where P_p is the pressure of mass flow and in our case $P_p=0$. \tilde{g} is the gravitational acceleration defined by the tidal gravity. δv is the change of velocity of mass transfer flow in a short time δt , and we have $\delta v = a \delta t$. Defining d to be the distance between the two stars, we have

$$\frac{1}{\delta v} = \frac{(d_1 d_2)^2}{(m_1 d_2^2 - m_2 d_1^2) \delta t}, \quad (45)$$

where d_1, d_2 are the distances from an infinitesimal fluid element to m_1 star m_2 star respectively. The mass change of two stars are due to tidal disruption [60]. According to above discussing we have $F_T = \rho \tilde{g} dV$, which is strongly

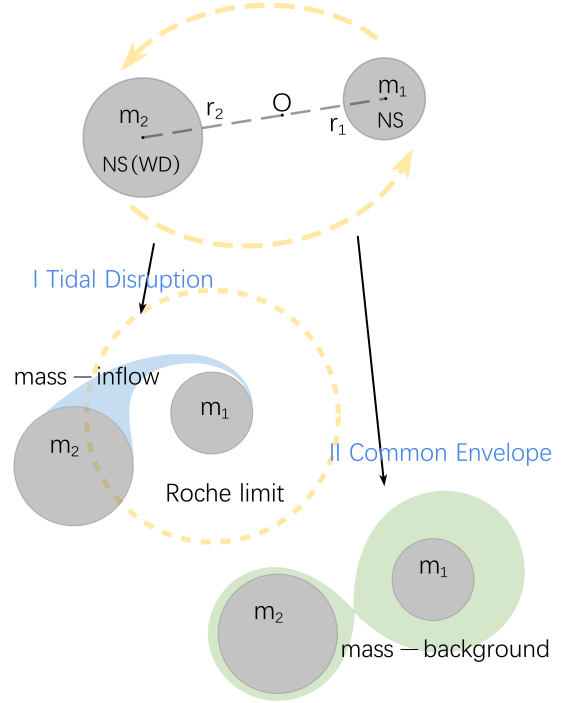


FIG. 2. At the top of the figure is the compact binaries in inspiral, where the mass of m_1 star is more compact than m_2 star. Below are two mass-transfer models, the left one is the case with tidal disruption only, and the right one is the case of common envelope evolution, which divides the mass-loss flow into mass-inflow and mass-background in the Roche lobe of m_1 star. The real astro process is usually the combination of those two.

related to the tidal gravity, and can be described as an analytical function

$$F_T = \frac{M\mu}{(d-R_0)^2} - \frac{M\mu}{d^2} = \frac{M\mu(2dR_0 - R_0^2)}{d^4 - 2d^3R_0 + R_0^2d^2}, \quad (46)$$

where R_0 is the radius of m_2 . Using tidal gravity as a mass transfer function, we then obtain the mass change in the system at any time interval

$$m'_1 = m_1 + \alpha \frac{m_1 m_2 R_0}{2(m_1 - m_2)(d - R_0)\delta t} \quad (47)$$

$$m'_2 = m_2 - \frac{m_1 m_2 R_0}{2(m_1 - m_2)(d - R_0)\delta t} \quad (48)$$

where $0 \leq \alpha \leq 1$ is the mass-inflow parameter, thus $m'_1 = \alpha m'_2$. In this section we set $\alpha = 1$, meaning the total mass of the binaries is conserved with no external accretion process.

When a static, spherically symmetric star with mass m in an external quadrupole tidal field ϵ_{ij} which is a function of F_T , it deforms as its varying quadrupole tensor Q_{ij} [60, 61].

$$g_{ij} = 1 - 2 \left[-\frac{m}{r} - \frac{3Q_{ij}}{2r^3} \left(\frac{x^i x^j}{r^2} - \frac{\delta_{ij}}{3} \right) + \frac{F_T}{2r} x^i x^j \right]. \quad (49)$$

The change of Weyl scalar is

$$\delta\psi_4 = -\frac{9(\pi M f)^{\frac{5}{3}}}{16\mu M^4} \left[\left(11\frac{m_1}{m_2} + \frac{M}{m_1} \right) \frac{1}{r\delta v} + 1 \leftrightarrow 2 \right]. \quad (50)$$

Defining $q' = m_2/m_1 = 1/q$, the evolution of inspiral semi-major axis and GW frequency are [62]

$$\frac{da}{dt} = -\frac{64\mu M^2 a^{-3}}{5(1-e^2)^{\frac{7}{2}}} \left(1 + \frac{73}{24}e^2 + \frac{37}{96}e^4 \right) - 2aC\frac{\dot{m}_2}{m_2}, \quad (51)$$

$$\frac{df}{dt} = \frac{96}{5}\pi^{\frac{8}{3}}m_1m_2M^{-\frac{1}{3}} + 3fC^{-1}\frac{\dot{m}_2}{m_2}, \quad (52)$$

$$C = [1 - \alpha q' - (1 - \alpha)\frac{q'}{q' + 1} - \alpha\sqrt{1 + q'}]^{-1}. \quad (53)$$

After adding the mass-transfer correction, we calculated the GWF changes produced by the NS-NS system and the NS-WD system.

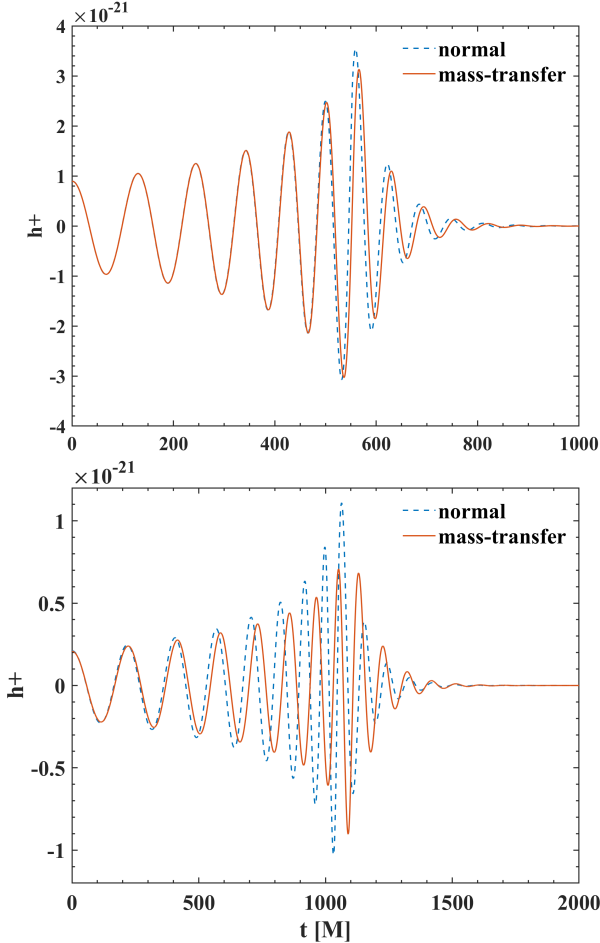


FIG. 3. The upper picture shows the little correction on inspiral GWF of NS-NS binaries with small q , R_{NS} , and Roche limit, while the lower shows the NS-WD case, where the shrink of strain peak and the delay of merger time is much more obvious, and the mass-transfer process also happens earlier

Besides the compactness of NSs, whose radii are about $R_{NS} \cong 3 \times 10^{-5} R_{\odot}$ meaning the tidal disruption can

only happen in a very close region, the tidal influence on inspiral GW itself is a small correction for $(2.0 + 1.4)M_{\odot}$ NS-NS binaries. Therefore we turn to establish a $(2.0 + 0.5)M_{\odot}$ NS-WD system with the radius of WD is $R_0 \cong 1 \times 10^{-2} R_{\odot}$. Plugging the corrected formula into the equations we solved in the last section, the results are shown in FIG.3.

In order to future investigate the underlying causes of the variation in GWF, we simultaneously plot the evolution of dynamical parameters of the $(2.0 + 0.5)M_{\odot}$ NS-WD system, including the radiation power, orbital eccentricity, and orbital radius. The radiation power increases significantly as it approaches the merger, so the natural logarithmic value is used as the vertical coordinate of FIG.4. The main difference appears in the late inspiral phase, when m_2 star moves within the Roche limit of m_1 star and before merger phase.

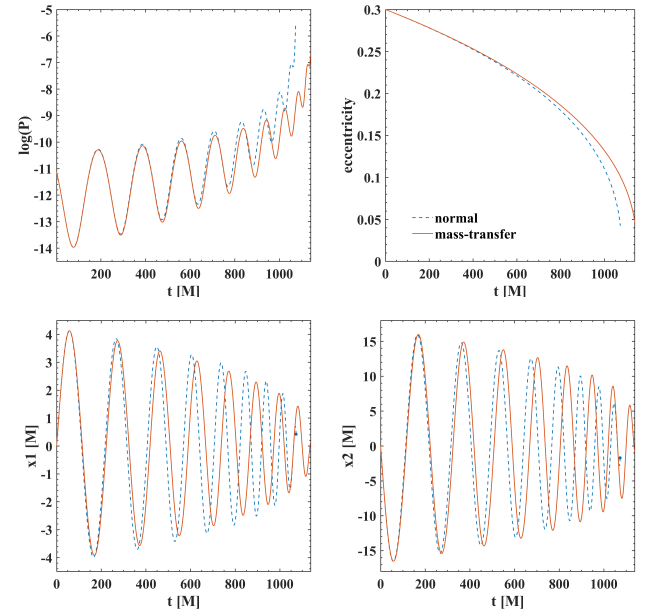


FIG. 4. Time evolution of each dynamical parameters of NS-WD binaries system with the mass-transfer correction. The blue points in the two figures of x_1 and x_2 (orbital radii of NS and WD) indicate merger without mass-transfer.

The figure shows that the radiation power of the system decreases after the mass-transfer correction, while the effect on the orbital eccentricity is not so obvious. The bottom left figure shows the orbital radius of the NS, whose orbital radius decreases more quickly receiving transferred mass, while the change on the WD is less clear.

C. Common Envelope

We consider that in addition to the direct mass-transfer flow between two stars [34, 55], a portion of the

mass-loss forms into a common envelope that wraps up the two stars as a mass-background in the Roche lobe of the NS. This mass is still part of the binary system but does not explicitly belongs to neither star, and because of its regular shape and symmetric mass distribution, we consider it as a third rotating non-spherically symmetric star.

The mass-background will be concentrated in the Roche lobe, whose radius [63] is

$$r_L(q) = \frac{0.49q^{2/3}}{0.6q^{2/3} + \ln(1 + q^{1/3})}. \quad (54)$$

We take ellipsoidal neutron stars as an analog to the common envelope [64]. The variation of the rotation period is influenced by the accretion process while emitting GWs with radiation power

$$P = \dot{E}_{GW} = -\frac{32}{5}I^2e^2\omega^6, \quad (55)$$

$$\omega = \left(\frac{5\dot{M}}{64I^2e^2}\sqrt{RR_A}\right)^{1/2}. \quad (56)$$

The ω indicates the angular velocity of neutron star spin, while I is the rotational moment of inertia, and R_A is Alvin Radius. Then we obtain the expression for h with both mass-background spin and the binary inspiral. Here $H(t)$ is the amplitude of the spin GW, which can be expanded to 3PN order [65] as

$$h_+ = h_+^{In} + H(t)e^{-im\phi_{orb}t}. \quad (57)$$

There will be dynamical friction [66, 67] when the m_2 star enters the common envelope that winds inside the NS Roche lobe. This friction will obstruct the motion of m_2 star and cause kinetic energy loss, making the binary merge more rapidly. However, this phenomenon mainly happens in the interaction between Galactic globular clusters and external stars. In our case, the frictional force is much weaker than the gravitational force and is negligible in the calculation.

In the case of the common envelope evolution, we need to calculate the mass that flows from m_2 to m_1 , and that becomes the mass-background. Here we introduce two parameters to describe the stability of mass-transfer in NS-WD systems.

$$\zeta_P = \partial \ln r_p / \partial \ln \dot{M}, \quad (58)$$

is associated with the adiabatic mass-radius r_p and

$$\zeta_L = \partial \ln r_L / \partial \ln \dot{M}. \quad (59)$$

Has to do with the NS Roche lobe radius r_L [68, 69]. When $\zeta_P - \zeta_L > 0$ we think it is a stable mass-transfer process. Furthermore, we can have the mass inflow parameter $\alpha = \delta m_1 / \delta m$, where δm is the mass-loss of WD and δm_1 is the mass-inflow to NS. It can also be written

as [62, 70]

$$\alpha \equiv \partial \ln \dot{m}_1 / \partial \ln r, \quad (60)$$

$$\alpha(\eta_w, \gamma) = \frac{1}{2}[1 - \eta_w\gamma + (-5\gamma^2 + 10\eta_w\gamma^2 + \eta_w^2\gamma^2 + 6\gamma)^{1/2}] / (-\gamma + 2\eta_w\gamma + 1), \quad (61)$$

where $\gamma = 5/3, 4/3$ is an adiabatic coefficient, and η_w is the winding efficiency parameter, which depends on factors such as the mass ratio, Keplerian orbital velocity, and the asymptotic wind velocity. For $\eta_w \sim 1$ this is a factor of $\vartheta < 1$ times smaller than the local dynamical time-scale, where ϑ is a function of mass ratio q .

We know that for a $(1.4 + 0.1)M_\odot$ NS-WD system, $\alpha \gtrsim 0.5$ of the WD mass-loss can be captured by its companion NS, while for $(1.4 + 1.25)M_\odot$ NS-WD system, the mass-inflow parameter α drops steeply to 5.4×10^{-4} [62]. The relation between α and q can be written in a more explicit form. Expanding η_w to the linear term of q , we can switch the above function into $\alpha(q, \gamma)$. In the following calculation, we set $\gamma = 5/3$. The results are shown in FIG.5. Here we apply NS-WD binaries with $q = 4$ and $\alpha = 0.1662$, and see the common envelope enhances the effect of mass transfer by a little bit, with weaker GW strain and more time delay.

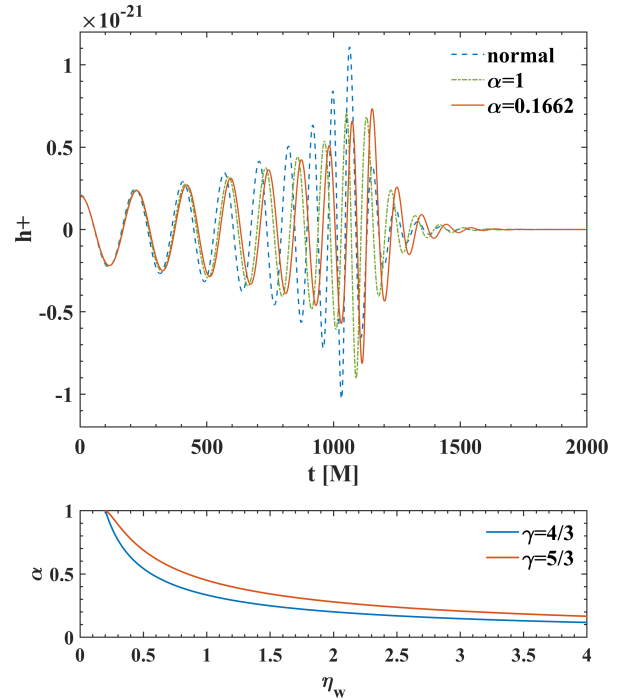


FIG. 5. The upper figure shows the GWs of NS-WD binaries with mass-inflow parameter α , we can see the decrease of GW strain and frequency reduction, which cause the delay of merger time. And the GWs of ringdown phase are depend on the merger momentum and frequency. The lower figure illustrates the mass-inflow parameter α function of η_w .

In FIG.7 we give the orbital trajectory of the NS-WD binaries with $q = 4$ and $\alpha = 0.1662$. Here we only

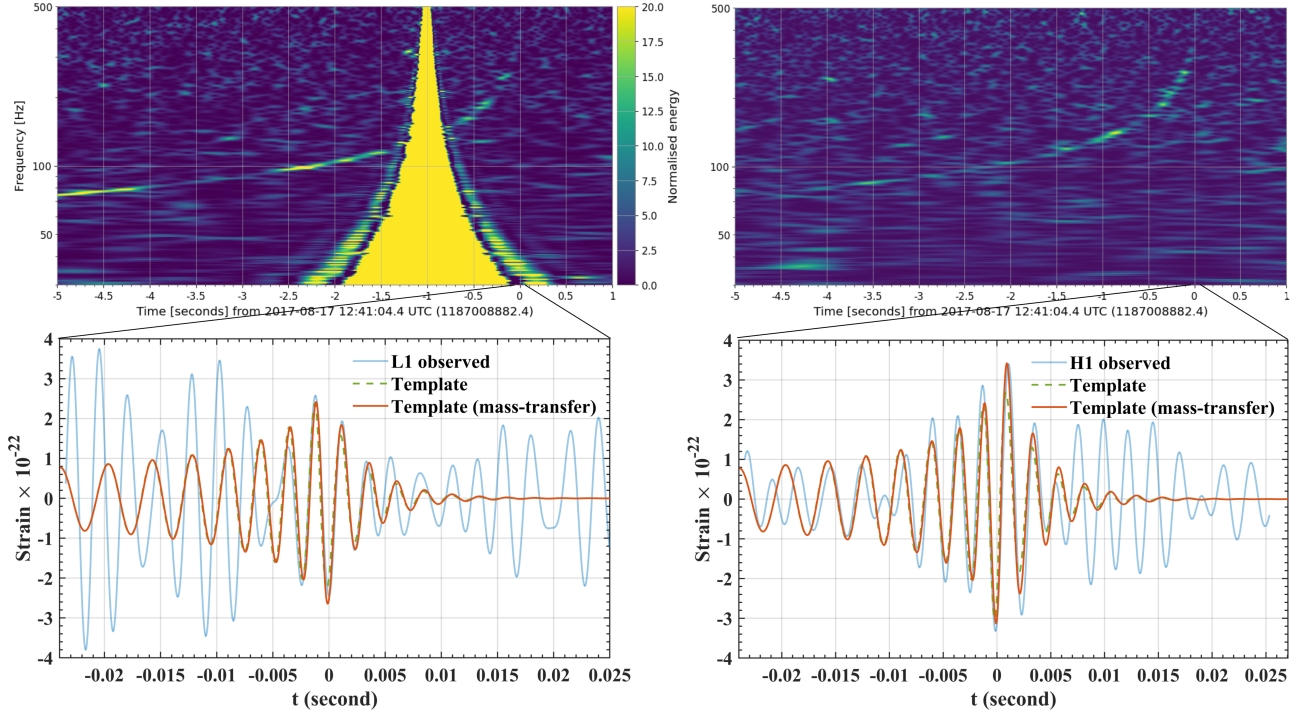


FIG. 6. The comparisons to the GW170817 data by LIGO [71, 72], which is labeled by blue lines. The top panels are the initial data drawn in the frequency domain, where we can see the chirp rising. The left one from L1 has encountered some technical issues showing as the peak-shaped image, which leads to the failure of further processing. This is why the corresponding signal below is severely distorted, where only the merger is readable. The precise fitting parameters are listed in TAB.I

TABLE I. The detection data and the initial parameters of numerical calculation of GW170817. \mathcal{M} is the chirp mass, M is the total mass, R is the distance from us, θ is the viewing angle, χ is the effective spin parameter, q is the mass ratio, and e is the eccentricity of orbit.

GW170817	$m_1(M_\odot)$	$m_2(M_\odot)$	$\mathcal{M}(M_\odot)$	$M(M_\odot)$	$R(\text{Mpc})$	$\theta(^{\circ})$	χ_{eff}	q	e
Detection data	$1.46^{+0.12}_{-0.10}$	$1.27^{+0.09}_{-0.09}$	$1.188^{+0.004}_{-0.002}$	$2.74^{+0.04}_{-0.01}$	40^{+7}_{-15}	≤ 56	$0^{+0.02}_{-0.01}$	$1.15^{+0.19}_{-0.15}$	-
Setting parameters	1.46	1.27	1.185	2.73	42	56	0	1.15	0.2

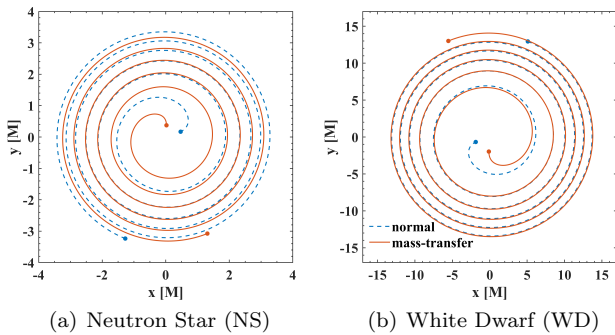


FIG. 7. In order to discuss the orbital differences caused by mass-transfer more clearly, we set the origin of both pictures fixed at the mass center of two stars, which is actually not stationary as the binary mass ratio changes. The time interval in the diagram is $t = 500 \sim 1000[M]$

present the part during $t = 500 \sim 1000[M]$, since the divergence between mass transfer trajectories and nor-

mal ones mainly arises at the latter phase of the inspiral. Owing to the delaying effect, the starting points of those two cases do not coincide and nor the endpoints of our illustration. There are more complex dynamical processes taking place as the two stars move too close to each other in the merger phase and the computation is cut off. However, we can still see the tendency of colliding from the diagrams.

From the discussion above we can intuitively see the prominent role that mass-transfer plays in the orbits evolution and GWF of NS-WD inspiral phase of binaries, especially the terminus when close to merge.

D. Match with the Template with GW170817

To verify our models, it is helpful to compare them with the actual data. Since no NS-WD signals have ever been detected, here we choose GW170817, the first NS-NS merger signal. This event occurred at GPS time

1187008882.43 = August 17 2017, 12:41:04.43 UTC, was widely observed by many electromagnetic bands simultaneously, and has a very high confidence level to be a NS-NS binary. Since the masses of the experimental signal are much more precise than the distance, we follow the given mass and set the distance and eccentricity to be fitting parameters. Our priority is to match the merger signal with the highest confidence, with turns out very well. The mismatch of the inspiral may come from the choice of initial velocities. Also, due to the frequency filter which would distort the low frequency inspiral, and the Livingston signal is scratched, the experimental data may not be very faithful, so this mismatch is preserved.

As for the post-merger waveform, we can see the unusual amplitude increasing in the reference data [73, 74]. This results from the small mass of NS-NS binary, that this part of the signal is beyond the LIGO's sensitivity and of very low confidence level [75]. Here we draw the black hole ringdown waveform, simply for completeness.

We obtained the data Gravitational Wave Open Science Center website, and let the whitened data pass a low-frequency filter to reduce the background noise [76]. We see that the binary orbiting frequency is around 400 Hz, and thus we portray the signals between [300 Hz, 500 Hz]. We set the merger time to be the origin and focus on the waveforms between $[-0.023$ s, 0.023 s], and the results are shown in FIG.6.

From the contrast above, the imitation of our models is generally valid to reach the expectations in practical terms.

E. Binary Systems with Different Mass Ratios

In the last section, we mainly discussed compact NS-WD binary systems with initial mass ratio $q = m_1/m_2 = 4$, and here we investigate a more general range of mass ratios, which are still commonly seen in actual cases [77, 78].

Taking $(2 + 0.5)M_\odot$, $(2 + 0.7)M_\odot$, and $(2 + 1.0)M_\odot$ NS-WD binaries as representatives illustrated in FIG.8. In addition to the effect on the Roche limit of NS, the variation on q also leads to variation on α .

In order to get the evolution information of $m_1(t)$ and $m_2(t)$, we plot the mass change curve in FIG.9. We can see that the mass-transfer occurs earlier for WDs with smaller masses, while it is very characteristic that the final masses of NSs are basically all similar, which is caused by the variation of the mass-loss δm_l and the mass-inflow parameter α . However, there is a significant difference in the lost mass of WDs. When m_2 gets heavier, the proportion $\delta m_l/m_2$ and mass loss δm_l both decrease. The step structure at the beginning of the mass change is due to the binary distance oscillating above and below the Roche limit with the changing of eccentricity, causing mass transfer happens intermittently. As the distance between NS and WD decreases, the mass-loss rate becomes larger.

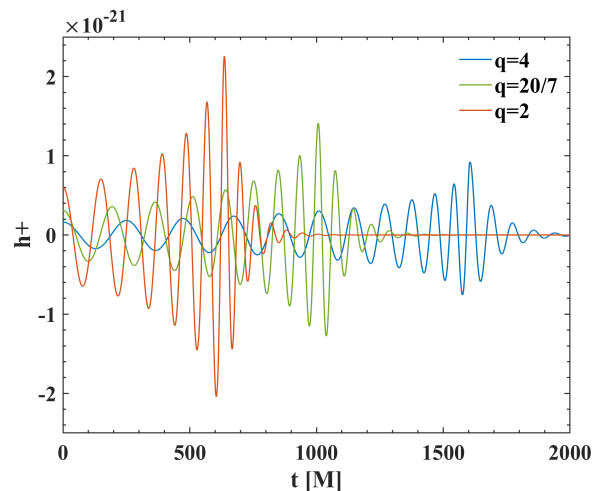


FIG. 8. Set the initial mass of WD $m_2 = 0.5, 0.7, 1.0M_\odot$ and $m_1 = 2.0M_\odot$, then get the mass ratio $q = 4, \frac{20}{7}, 2$ and distance $d = 23R_\odot$. As q decreases, the merger time is bought forward and the GW strain grows intensively.

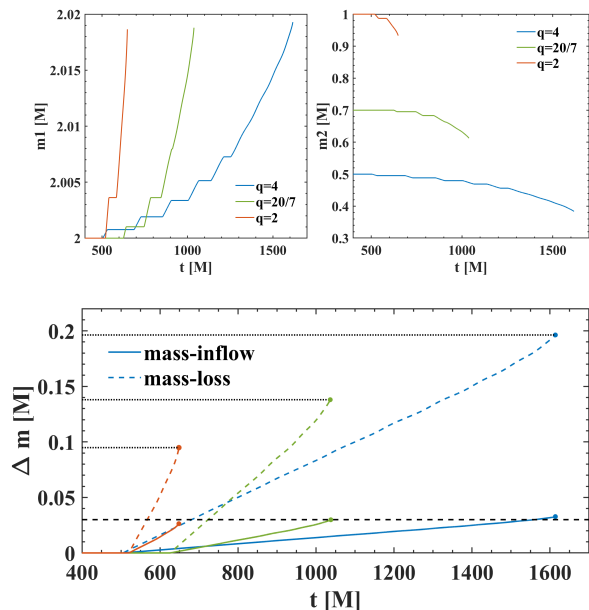


FIG. 9. In different NS-WD systems, we get a nonlinear result as the mass ratio q decreases. This is due to the competition of following two effects. One is the faster radial velocity leading to earlier entering to the Roche limit. The other is the shrinking of Roche limit of the primary star, extending the distance to enter. The mass-transfer of $q = 1$ occurs between that of $q = 0.7$ and $q = 0.5$. As the lower figure demonstrates, bigger percentage of mass tends to form common envelope as m_2 decrease.

The final mass of NS-WD, $\delta m/m$ and mass-inflow parameter α are listed in TAB.II, where $m_i^{(f)}$ is the final mass of m_i and $m_2^{(0)}$ is the initial mass of m_2 . For the WDs mass at $0.5 \sim 1.0M_\odot$, the mass-loss ratio changes

from 0.395 to 0.095, showing the stronger mass-transfer process with the smaller mass WD. In [79] Metzger found accretion ratios of $10^{-4} \sim 10^{-1} M_{\odot}/s$ for tidal disruption of a WD by a NS or a black hole, consistent in our results well.

TABLE II. Mass-transfer of NS-WD binaries

NS-WD	$m_1^{(f)}$	$m_2^{(f)}$	δm_l	$\delta m_l/m_2^{(0)}$	α
$(2 + 0.5)M_{\odot}$	2.033	0.383	0.196	0.395	0.166
$(2 + 0.7)M_{\odot}$	2.030	0.612	0.138	0.199	0.215
$(2 + 1.0)M_{\odot}$	2.026	0.932	0.095	0.095	0.279

We calculated the orbit of $(2+0.7)M_{\odot}$ and $(2+1.0)M_{\odot}$ NS-WD binaries in FIG. 10, the winding radii ratio of WD and NS is proportional to q . When q is large, the trajectory of the binaries is more inclined to the situation where WD winds around while the NS only swings a bit at the center. In a more extreme case, the NS would tend to be stable, which takes the longest time to merge. In the case of NS-NS systems, the binary stars have similar masses and radii, and their trajectories will exhibit a centrosymmetric pattern.

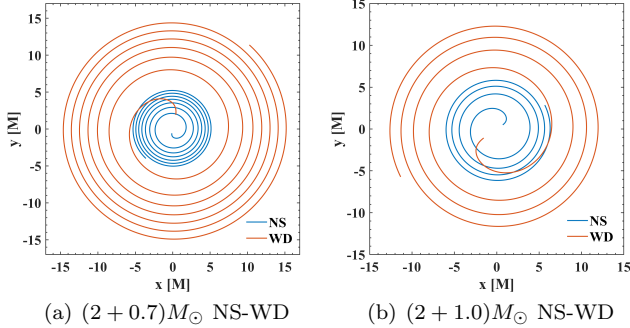


FIG. 10. The calculation of the orbit of NS-WD binaries. The initial distance of the binary star is $d = 23R_{\odot}$, and the orbits of $t = 500 \sim 1000[M]$ is shown in the figure. When the mass ratio q of the binaries decrease, the orbit radius become more similar.

In summary, as the mass of WD increases the binaries tend to merge more quickly and the number of turns of rotations decreases significantly. At the same time, the increased mass of the stars leads to an increase in the changing rate of the mass quadrupole tensor, while the gravitational radiation power and GW strain during the inspiral also increase.

Furthermore, in order to check the convergence of the model in the whole mass interval, we discussed m_2 going from $0.4M_{\odot}$ to $1.2M_{\odot}$ in FIG. 11 whose mass ratio decreases exponentially, where the general white-dwarf mass is most concentrated in $0.493M_{\odot}$ and $1.05M_{\odot}$ [80]. When m_2 approach $m_1 = 2M_{\odot}$, this system approaches

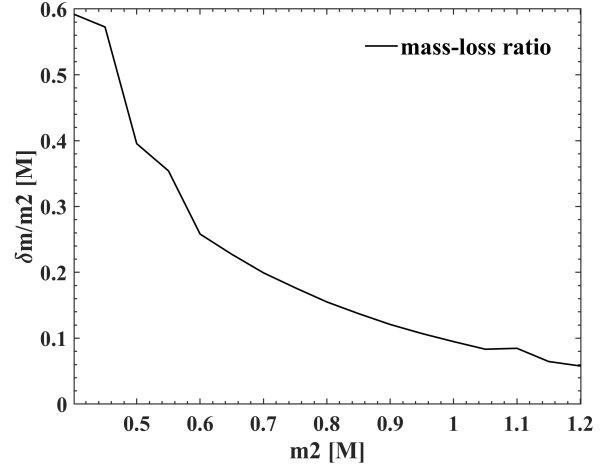


FIG. 11. Mass of WD changes form $0.4M_{\odot}$ to $1.2M_{\odot}$, which is almost the mass range of a white dwarf in detection. When $m_2 \gtrsim 0.45M_{\odot}$, $\delta m/m_2$ varies exponentially with m_2 , and the change ratio of $\delta m/m_2$ becomes smaller and eventually stables at about 0.6 when the mass reduces to smaller than $0.4M_{\odot}$.

to NS-NS system with basically no mass-transfer. When the WD mass reduces to $0.45M_{\odot}$, the mass-loss ratio reaches 0.5725, and the mass-loss change rate of $\delta m/m_2$ becomes smaller and stables at about 0.6 while the mass reduces to smaller than $0.4M_{\odot}$, which also ensures the convergence when the WD mass is small.

V. CONCLUSIONS

For the tidal disruption type of mass-transfer, the overall variations of NS-NS binaries' GWs are small, while a larger change occurs on the NS-WD binaries with the mass-loss, which is divided into mass-background and mass-inflow. We have theoretically derived the equation for mass-transfer by tidal gravity, and then added the mass-inflow parameter α to calculate the various types of mass evolution in the binaries and their corresponding GWs. We set the massive NS $m_1 = 2M_{\odot}$ and WD $m_2 = 0.4 \sim 1.2M_{\odot}$, then obtained $\alpha = 0.1393 \sim 0.3204$ and mass-loss $\delta m/m_2 = 0.5923 \sim 0.0578$. These results are consistent with the current observation data, and the calculation is convergent throughout the mass ranges of WD.

The dynamical evolution of a NS-WD system involves more physical processes than a binary mass point system. We effectively and reasonably simplified the independent variables and mass distribution, and gave the GWs in various cases by different theoretical bases, which constitute a more comprehensive library of GWs templates. When using the post-Newton approximation to calculate the mass-transfer correction, since the NS-NS binaries have no prominent effect on the waveform, we focused

on the NS-WD binaries, which have larger q and Roche limit. This result is due to the boundedness of post-Newtonian approximation which loses efficacy at the merger phase when complex dynamical processes emerge.

As a future study, numerical-relativity method can be applied to cope with merger phase, allowing to improve our accuracy and various mass-transfer model can be probed in. Also, with more experimental data being detected, we can further test our simulations by comparisons. As the precision and sensitivity improve, we may be able to find more inspiral status information like

the orbital eccentricity and velocity in running of next-generation observatories using redundant fitting parameters.

VI. ACKNOWLEDGMENTS

This work is partially supported by the National Key Research and Development Program of China (Grant No. 2020YFC2201503).

-
- [1] T. Regimbau and S. A. Hughes, *Phys. Rev. D* **79**, 062002 (2009).
 - [2] B. Liu and D. Lai, *The Astrophysical Journal* **924**, 127 (2022).
 - [3] V. Baibhav, E. Berti, D. Gerosa, M. Mapelli, N. Giacobbo, Y. Bouffanais, and U. N. Di Carlo, *Phys. Rev. D* **100**, 064060 (2019).
 - [4] E. Berti, L. Gualtieri, M. Horbatsch, and J. Alsing, *Phys. Rev. D* **85**, 122005 (2012).
 - [5] X.-H. Zhang, S.-D. Zhao, S. D. Mohanty, and Y.-X. Liu, *Phys. Rev. D* **106**, 102004 (2022).
 - [6] S. Babak, R. Balasubramanian, D. Churches, T. Cokelaer, and B. S. Sathyaprakash, *Classical and Quantum Gravity* **23**, 5477 (2006).
 - [7] T. Cokelaer, *Classical and Quantum Gravity* **24**, 6227 (2007).
 - [8] M. Shibata, K. Kyutoku, T. Yamamoto, and K. Taniguchi, *Phys. Rev. D* **85**, 127502 (2012).
 - [9] M. Shibata, K. Kyutoku, T. Yamamoto, and K. Taniguchi, *Phys. Rev. D* **79**, 044030 (2009).
 - [10] T. Wagg, F. S. Broekgaarden, S. E. de Mink, N. Frankel, L. A. C. van Son, and S. Justham, *The Astrophysical Journal* **937**, 118 (2022).
 - [11] Y. Kang, C. Liu, and L. Shao, *The Astronomical Journal* **162**, 247 (2021).
 - [12] Z. Fan, L. Zhao, S. Cao, J. Peng, H. Ji, Z. Zhu, S. Wei, Y. Mo, H. Chen, and D. Ma, *Classical and Quantum Gravity* **39**, 195017 (2022).
 - [13] S. Kawamura and Ando, *Progress of Theoretical and Experimental Physics* **2021** (2021).
 - [14] B. McKernan, K. E. S. Ford, and R. O'Shaughnessy, *Monthly Notices of the Royal Astronomical Society* **498**, 4088 (2020).
 - [15] C. Hamilton and R. R. Rafikov, *The Astrophysical Journal* **939**, 48 (2022).
 - [16] G. M. Kremer, *Research in Astronomy and Astrophysics* **22**, 125009 (2022).
 - [17] L. Blanchet, S. Detweiler, A. Le Tiec, and B. F. Whiting, *Phys. Rev. D* **81**, 064004 (2010).
 - [18] I. Futamase, Toshifumi, *Living Reviews in Relativity* (2007).
 - [19] T. Rainsford, *General Relativity and Gravitation* (2000).
 - [20] D. Bini and T. Damour, *Phys. Rev. D* **87**, 121501 (2013).
 - [21] G. Cho, A. Gopakumar, M. Haney, and H. M. Lee, *Phys. Rev. D* **98**, 024039 (2018).
 - [22] H. W. B. T. Cai R G, Cao Z J, *hin Sci Bull* (2016).
 - [23] S. Tanay, M. Haney, and A. Gopakumar, *Phys. Rev. D* **93**, 064031 (2016).
 - [24] J. H. Krolik and I. Linial, *The Astrophysical Journal* **941**, 24 (2022).
 - [25] T. R. Li Yaguang, Bedding, *Nature Astronomy* (2022).
 - [26] H.-L. Chen, T. M. Tauris, X. Chen, and Z. Han, *The Astrophysical Journal* **925**, 89 (2022).
 - [27] Y.-J. Huang, *Ph.D. thesis*, University of Science and Technology of China (2022).
 - [28] Y.-J. Huang, L. Baiotti, T. Kojo, K. Takami, H. Sotani, H. Togashi, T. Hatsuda, S. Nagataki, and Y.-Z. Fan, *Phys. Rev. Lett.* **129**, 181101 (2022).
 - [29] P. S. PALMER, *Nature* (1954).
 - [30] R.-X. Yang, F. Xie, and D.-J. Liu, *Universe* **8** (2022).
 - [31] S. Mougiakakos, M. M. Riva, and F. Vernizzi, *Phys. Rev. Lett.* **129**, 121101 (2022).
 - [32] R. G. Izzard, P. D. Hall, T. M. Tauris, and C. A. Tout, *Proceedings of the International Astronomical Union* **7**, 95–102 (2011).
 - [33] M. E. Beer, L. M. Dray, A. R. King, and G. A. Wynn, *Monthly Notices of the Royal Astronomical Society* **375**, 1000 (2007).
 - [34] T. L. S. Wong and L. Bildsten, *The Astrophysical Journal* **923**, 125 (2021).
 - [35] N. Soker, *Monthly Notices of the Royal Astronomical Society* **509**, 2836 (2021).
 - [36] D. G. Figueroa, J. Garcia-Bellido, and A. Rajantie, *Journal of Cosmology and Astroparticle Physics* **2011**, 015 (2011).
 - [37] T. Mora and C. M. Will, *Phys. Rev. D* **69**, 104021 (2004).
 - [38] L. E. Kidder, *Phys. Rev. D* **52**, 821 (1995).
 - [39] H. Tagoshi, A. Ohashi, and B. J. Owen, *Phys. Rev. D* **63**, 044006 (2001).
 - [40] L. Blanchet, A. Buonanno, and G. Faye, *Phys. Rev. D* **75**, 049903 (2007).
 - [41] X. Wu, L. Mei, G. Huang, and S. Liu, *Phys. Rev. D* **91**, 024042 (2015).
 - [42] D. Bini and T. Damour, *Phys. Rev. D* **96**, 064021 (2017).
 - [43] M. Ebersold, Y. Boetzel, G. Faye, C. K. Mishra, B. R. Iyer, and P. Jetzer, *Phys. Rev. D* **100**, 084043 (2019).
 - [44] K. Cannon, C. Hanna, and D. Keppel, *Phys. Rev. D* **88**, 024025 (2013).
 - [45] B. san Sun, *Ph.D. thesis*, Huazhong University of Science and Technology (2015).
 - [46] R. Cotesta, G. Carullo, E. Berti, and V. Cardoso, *Phys. Rev. Lett.* **129**, 111102 (2022).
 - [47] Y. Boetzel, C. K. Mishra, G. Faye, A. Gopakumar, and B. R. Iyer, *Phys. Rev. D* **100**, 044018 (2019).
 - [48] S. A. Hughes, A. Apte, G. Khanna, and H. Lim, *Phys. Rev. Lett.* **123**, 161101 (2019).

- [49] F. Echeverria, [Phys. Rev. D **40**, 3194 \(1989\)](#).
- [50] A. R. King and U. Kolb, [Monthly Notices of the Royal Astronomical Society **305**, 654 \(1999\)](#).
- [51] E. T. Newman and R. Penrose (1962).
- [52] S. Babak, H. Fang, J. R. Gair, K. Glampedakis, and S. A. Hughes, [Phys. Rev. D **75**, 024005 \(2007\)](#).
- [53] L. Blanchet, [Living Reviews in Relativity \(2002\)](#).
- [54] M. Maggiore, *Gravitational Waves Vol 1* (Oxford, 2008).
- [55] P. Hölscher and D. J. Schwarz, [Phys. Rev. D **99**, 084005 \(2019\)](#).
- [56] P. C. Peters and J. Mathews, [Phys. Rev. **131**, 435 \(1963\)](#).
- [57] P. C. Peters, [Phys. Rev. **136**, B1224 \(1964\)](#).
- [58] A. Gaull, [Multibody System Dynamics \(2019\)](#).
- [59] N. Nadirashvili, [Archive for Rational Mechanics and Analysis \(2013\)](#).
- [60] E. E. Flanagan and T. Hinderer, [Phys. Rev. D **77**, 021502 \(2008\)](#).
- [61] K. S. Thorne, [Phys. Rev. D **58**, 124031 \(1998\)](#).
- [62] S. Yu, Y. Lu, and C. S. Jeffery, [Monthly Notices of the Royal Astronomical Society **503**, 2776 \(2021\)](#).
- [63] P. P. Eggleton, [Astrophysical Journal \(1983\)](#).
- [64] S. L. Shapiro and S. A. Teukolsky, *Black Holes, White Dwarfs and Neutron Stars* (Wiley-Interscience, 1983).
- [65] K. G. Arun, A. Buonanno, G. Faye, and E. Ochsner, [Phys. Rev. D **84**, 049901 \(2011\)](#).
- [66] M. Brockamp, A. H. W. Küpper, I. Thies, H. Baumgardt, and P. Kroupa, [Monthly Notices of the Royal Astronomical Society **441**, 150 \(2014\)](#).
- [67] S. Adhikari, N. Dalal, and J. Clampitt, [Journal of Cosmology and Astroparticle Physics **2016** \(07\), 022](#).
- [68] F. D’Antona, I. Mazzitelli, and H. Ritter, [Astronomy and Astrophysics **225**, 391 \(1989\)](#).
- [69] P. P. Eggleton, [The Astrophysical Journal **268**, 368 \(1983\)](#).
- [70] B. Margalit and B. D. Metzger, [Monthly Notices of the Royal Astronomical Society **461**, 1154 \(2016\)](#).
- [71] B. P. Abbott, R. Abbott, and T. D. e. Abbott, [Phys. Rev. Lett. **119**, 161101 \(2017\)](#).
- [72] B. P. Abbott, R. Abbott, T. D. Abbott, and et.al., [Phys. Rev. X **9**, 011001 \(2019\)](#).
- [73] E. E. Flanagan and S. A. Hughes, [Phys. Rev. D **57**, 4566 \(1998\)](#).
- [74] E. E. Flanagan and S. A. Hughes, [Phys. Rev. D **57**, 4535 \(1998\)](#).
- [75] M. Agathos, F. Zappa, S. Bernuzzi, A. Perego, M. Breschi, and D. Radice, [Phys. Rev. D **101**, 044006 \(2020\)](#).
- [76] B. P. Abbott, R. Abbott, T. D. Abbott, and et.al., [Classical and Quantum Gravity **37**, 055002 \(2020\)](#).
- [77] A. H. Nitz and Y.-F. Wang, [Phys. Rev. Lett. **126**, 021103 \(2021\)](#).
- [78] P. R. Brady and S. A. Hughes, [Phys. Rev. Lett. **79**, 1186 \(1997\)](#).
- [79] B. D. Metzger, [Monthly Notices of the Royal Astronomical Society **419**, 827 \(2011\)](#).
- [80] A. D. Romero, S. O. Kepler, S. R. G. Joyce, G. R. Lauffer, and A. H. Corsico, [Monthly Notices of the Royal Astronomical Society **484**, 2711 \(2019\)](#).